HHS Public Access

Author manuscript

J Neuroendocrinol. Author manuscript; available in PMC 2020 October 13.

Published in final edited form as:

J Neuroendocrinol. 2019 October ; 31(10): e12791. doi:10.1111/jne.12791.

Activation of Alpha-1 Adrenergic Receptors Increases Cytosolic Calcium in Neurons of the Paraventricular Nucleus of the Hypothalamus

William J. Milanick[1,3], **Luis Polo-Parada**[2,3], **Heather A. Dantzler**[1,3], **David D. Kline**[1,3]

[1]Department of Biomedical Sciences, University of Missouri, Columbia MO 65211

[2]Department of Medical Pharmacology and Physiology, University of Missouri, Columbia MO 65211

[3]Dalton Cardiovascular Research Center, University of Missouri, Columbia MO 65211

Abstract

Norepinephrine (NE) activates adrenergic receptors (ARs) in the hypothalamic paraventricular nucleus (PVN) to increase excitatory currents, depolarize neurons, and ultimately augment neuro-sympathetic and endocrine output. Such cellular events are known to potentiate intracellular calcium ($[Ca^{2+}]_i$), however, NE's role in modulating $[Ca^{2+}]_i$ in PVN neurons and the mechanisms by which this may occur is unclear. We evaluated the effects of NE on $[Ca^{2+}]_i$ of acutely isolated PVN neurons using fura-2 imaging. NE induced a slow increase in $[Ca^{2+}]_i$ compared to aCSF vehicle. NE-induced Ca^{2+} elevations were mimicked by the α_1-AR agonist phenylephrine (PE) but not α_2-AR agonist clonidine (CLON). NE and PE, but not CLON, also increased the overall number of neurons that increase $[Ca^{2+}]_i$ (i.e., responders). Elimination of extracellular Ca^{2+} or intracellular endoplasmic reticulum Ca^{2+} stores abolished the increase in $[Ca^{2+}]_i$ and reduced responders. Blockade of voltage-dependent Ca^{2+} channels abolished the α_1-AR induced increase in $[Ca^{2+}]_i$ and number of responders, as did inhibition of PLC, PKC, and IP_3 receptors. Spontaneous phasic Ca^{2+} events, however, were not altered by NE, PE, or CLON. Repeated K^+-induced membrane depolarization produced repetitive $[Ca^{2+}]_i$ elevations. NE and PE increased baseline Ca^{2+}, yet NE decreased the peak amplitude. CLON also decreased peak amplitude but did not affect baseline $[Ca^{2+}]_i$. Together these data suggest receptor-specific influence of α_1 and α_2 receptors on the various modes of calcium entry in PVN neurons. They further suggest Ca^{2+} increase via α_1-ARs is co-dependent on extracellular Ca^{2+} influx and intracellular Ca^{2+} release, possibly via a PLC-mediated signaling cascade.

Keywords

Synaptic Transmission; Catecholamine Signaling; Blood Pressure Control; Adrenergic Receptors

Corresponding author and address: David D. Kline, Ph.D., Department of Biomedical Sciences, Dalton Cardiovascular Research Center, University of Missouri, 134 Research Park Dr. Columbia, MO 65211, USA, klinedd@missouri.edu, Phone: +1-573-884-0505.

Author contributions:

WJM, LPP and DDK designed the study. WJM and HAD performed the experiments and analyzed the data. WJM prepared figures and drafted the manuscript. All authors interpreted the data, edited the manuscript and approved final version.

Disclosures: None

INTRODUCTION

The hypothalamic paraventricular nucleus (PVN) is an integrative nucleus critical to producing the appropriate physiological response to a variety of stressors and stimuli, including during hypoxic exposure and chemoreflex activation. For instance, hypoxia increases PVN FOS expression indicative of elevated neuronal activity, including in those neurons that express corticotropin-releasing hormone (CRH), vasopressin (AVP), and oxytocin (OT), as well as those that project to the brainstem nucleus tractus solitarii (nTS) (1–4). These activated neurons are likely functionally important as inhibition or elimination of the PVN reduces the respiratory and pressor response to chemoreflex activation and hypoxia (5–7). Hypoxia also activates other nuclei that innervate the PVN including the nTS, the first central site for chemoreflex processing, as well as the ventrolateral medulla (VLM) and locus coeruleus (8–10). Of these FOS-activated PVN-projecting nTS and VLM neurons, a large proportion are catecholaminergic. Such ascending PVN-projecting catecholaminergic fibers innervate neuroendocrine magnocellular and autonomic and neuroendocrine parvocellular neurons (11–15), and contribute to hypoxia-induced CRH release from the PVN (16).

Within the PVN, catecholaminergic inputs primarily release norepinephrine (NE) (11–13, 17, 18) which binds to one or more adrenergic receptors (AR) (19, 20). Several AR's are located within the PVN, including the alpha-1 (α_1) and alpha-2 (α_2) ARs in magnocellular and parvocellular regions (19, 21–23), specifically on CRH and AVP containing neurons, and beta-2 (β_2) receptors (24). Exposure of PVN magnocellular neurons to NE induces membrane depolarization and an increase in excitatory postsynaptic potentials, a response due to activation of α_1-ARs (25, 26). PVN parvocellular neurons exposed to NE exhibit both inhibitory and excitatory effects, with α_1-AR activation increasing action potential discharge, EPSP frequency, and in some cases direct depolarization of neuronal membranes, whereas α_2-AR activation decreases action potential discharge (25, 27–30). Functionally, increased NE in the PVN increases AVP, CRH, and OT secretion (20, 31–34).

Outside of NE's effect on synaptic transmission to parvocellular and magnocellular neurons, less is known as to what other functions NE has in the PVN. In other hypothalamic nuclei including the SON, NE increases intracellular Ca^{2+} ($[Ca^{2+}]_i$) via α_1-AR mediated pathways (35–38). In the nTS, α_1-AR activation induces neuronal $[Ca^{2+}]_i$ oscillations and increased excitation (39). Given the presence of adrenergic receptors in the PVN (17, 18, 40), catecholaminergic nTS neurons that innervate the PVN (11, 12), and the importance of $[Ca^{2+}]_i$ on cellular function; including neurotransmitter release, membrane potential, and gene and protein function (41), we examined the influence and mechanism by which NE modulates $[Ca^{2+}]_i$ in PVN neurons. In the present study, we demonstrate αARs play a profound, receptor-specific influence on calcium entry modes.

MATERIALS and METHODS

Experimental Animals.

Male Sprague-Dawley rats 3–5 wk in age were used (n=44). Rats where housed under 12 h light-dark cycle (22°C, 40% humidity) and given food and water *ad libitum* in an Association for Assessment and Accreditation of Laboratory Animal Care certified animal care center at the Dalton Cardiovascular Research Center. The Animal Care and Use Committee of the University of Missouri approved all animal protocols.

Acute PVN neuron isolation.

Neurons were isolated similar to our previously established protocols (42). Rats anesthetized with 5% isoflurane were decapitated and their forebrains were rapidly removed and placed into ice-cold high Mg^{2+} low Ca^{2+} cutting artificial cerebrospinal fluid (cutting aCSF, in mM: 124 NaCl, 3 KCl, 1.2 NaH_2PO_4, 1.2 $MgSO_4$, 25 $NaHCO_3$, 11 D-Glucose, 0.4 L-Ascorbic Acid, 1 $CaCl_2$, 2 $MgCl_2$, bubbled with 95% O_2 5% CO_2, pH 7.3–7.4, 295–305 mOsm). The hypothalamus was blocked based on the rostral-caudal landmarks of the optic tract. Coronal slices (~360 μm) containing the PVN were generated with a vibratome (VT1000S, Leica) in ice-cold cutting aCSF. PVN slices were transferred to 2 ml ice-cold Hibernate A medium (BrainBits, Springfield, IL) with added B-27 Supplement (Life Technologies, Burlington, ONT) and GlutaMAX (Invitrogen, Carlsbad, CA; HABG: 50 ml Hibernate A, 1 ml B-27 Supplement, 125 μl GlutaMAX). Using a dissecting scope and a 1 mm tissue punch (EMS-Core, Electron Microscopy Sciences, Hatfield, PA), PVN tissue lateral to the 3rd ventricle and medial to the magnocellular subregion was isolated, placed in 2 ml HABG and incubated for 8 min in a shaking water bath at 30°C and 170 rpm. The tissue was then transferred to 6 ml Hibernate A without $CaCl_2$ (BrainBits) with 34 U/ml papain (Worthington, Lakewood, NJ) and further incubated for 30 min at 30°C and 170 rpm. Papain digestion was terminated via tissue transfer to 2 ml of trituration solution: 15 ml HABG, 15 mg Ovomucoid (Worthington), 15 mg Bovine Serum Albumin (Sigma, Saint Louis, MO) and allowed to rest at 22°C for 5 min. Neurons were manually isolated using fire-polished glass pipets of decreasing tip diameter followed by passage through a 40 μm cell strainer to minimize cell debris. The cell suspension was spun down (70 g, 4 min), the supernatant discarded, and the resulting pellet reconstituted in ~100 μl Neurobasal-A medium [48 ml Neurobasal-A (Life Technologies), 1 ml B-27 Supplement, 500 μl Penicillin-Streptomycin-Neomycin (Life Technologies), 125 μl GlutaMAX, 50 μl Mito+ Serum Extender (Corning, Corning, NY), 50 μl Nerve Growth Factor (Chemicon International, Temecula, CA)]. The cell resuspension was placed on Poly-D-Lysine (100 μg/ml, Sigma) treated 15 mm glass coverslips, 20 μl per coverslip, and allowed to adhere for 2 h in the incubator (37°C, 5% CO_2). After 2 h the cells were flooded with 2 ml Neurobasal-A medium and returned to the incubator for at least 1 h before imaging.

Fura-2 calcium imaging.

All neurons were imaged as previously (42) on the same day as isolation. Fura-2 AM ratiometric dye (Life Technologies) was used to monitor $[Ca^{2+}]_i$,. All incubations and washes occurred in the dark incubator. Fura-2 AM (50 μg) was dissolved in 50 μl DMSO to create a 1 mM stock solution. Cells were loaded in 1 ml Neurobasal-A medium that

contained 1 μM fura-2 AM dye and 0.01% Pluronic F-127 (Sigma). Cells were subsequently washed twice in 1 ml Neurobasal-A medium (7 min each). A third wash occurred in imaging aCSF (in mM: 137 NaCl, 5.4 KCl, 1 $MgCl_2$, 2 $CaCl_2$, 0.33 NaH_2PO_4, 10 D-Glucose, 10 HEPES, pH 7.3–7.4, 295–305 mOsm) that was used throughout the subsequent protocols. The coverslip was mounted in a superfusion chamber, submerged with 0.5 ml aCSF, mounted on an Olympus IX71 microscope and superfused at ~4 μl/s.

A PolyChrome V (Till Photonics, Graefelfing, Germany) provided light at 340 and 380 nm to excite the fura-2 dye. An Olympus UAPON 20XW340 ×20 water immersion objective was used to visualize cells. Differential interference contrast (DIC) bright field images were acquired at the beginning and end of each experiment and fluorescent (510 nm emission) images were acquired at an image rate of either 20 images per min (one image every 3 s) or 12 images per min (one image every 5 s) with a Q-Imaging Regita Exi 12-bit camera and μManager 1.4 (Open Imaging).

Drugs and Protocols.

To examine the influence of adrenergic receptor (AR) activation on depolarization-induced Ca^{2+} increase, neurons were repeatedly depolarized with high K^+ depolarizing solution (K^+, in mM: 86 NaCl, 55.4 KCl, 1 $MgCl_2$, 0.33 NaH_2PO_4, 10 D-Glucose, 10 HEPES, 2 $CaCl_2$, pH 7.3–7.4, 295–305mOsm). Neurons were depolarized five times for 20 s each, with intermittent 5 min washes of imaging aCSF (Fig. 1A). Initial experiments demonstrated the third (K^+ 3, black in Fig. 1A), fourth (K^+ 4, blue in Fig. 1A) and fifth depolarization-induced increases, or peaks, were consistent under aCSF control conditions, and thus were used to examine the influence of AR activation on depolarization-induced Ca^{2+} entry. AR agonist or its vehicle (treatment) was bath applied in the wash between K^+ 3 and K^+ 4 depolarization. AR agonists included the general AR agonist norepinephrine (NE, Sigma, 100 μM), the α_1-AR agonist phenylephrine (PE, Sigma, 10 μM), and α_2-AR agonist clonidine (CLON, Sigma, 10 μM). Depolarization five (K^+ 5, Fig. 1A) confirmed the cell remained viable after AR agonist or vehicle application.

To examine the influence of AR activation on resting internal Ca^{2+} concentration ($[Ca^{2+}]_i$), and the potential pathways of action independent of K^+-induced depolarization, neurons were exposed to 5 min of imaging aCSF (control, black in Fig. 1B) followed by either NE, PE, or CLON alone (5 min agonist treatment, red in Fig. 1B) or in the presence of specific blockers. All blockers, with the exception of $CdCl_2$, were bath applied for 5 or more min prior to NE, PE, or CLON and remained present throughout the experiment. Blocker alone was considered the control period for the agonist application. The following blockers were used based on previous reports (42): Prazosin, an α_1-AR antagonist (PRA, Sigma, 10 μM, applied 5 min prior to agonist treatment), 0 mM Ca^{2+} solution ($[Ca^{2+}]_o$ Ø, in mM: 136 NaCl, 5.4 KCl, 2.8 $MgCl_2$, 0.33 NaH_2PO_4, 10 D-Glucose, 10 HEPES, pH 7.3–7.4, 295–305 mOsm), eliminates extracellular Ca^{2+} source (10 min exposure prior to agonist treatment); $CdCl_2$, a general Ca^{2+} channel blocker (GCC Ø, Sigma, 100 μM, applied with agonist or vehicle without pre-application to avoid Cd^{2+} induced fluorescence)(42); thapsigargin, a sarcoplasmic/endoplasmic reticulum Ca^{2+} ATPase inhibitor (SERCA Ø, Sigma, 1 μM, 1 h SERCA Ø incubation prior to fura-2 loading, SERCA Ø present in loading and all

successive solutions); U73122, a phospholipase C inhibitor (PLC Ø, Tocris, Bristol, UK, 10 μM, 10 min exposure prior to treatment)(39); Chelerythrine chloride, a protein kinase C inhibitor (PKC Ø, Tocris, 10 μM, 10 min exposure prior to treatment)(39); Xestospongin C, an inositol triphosphate receptor antagonist (IP_3R Ø, Tocris, 1 μM, 20 min exposure prior to treatment)(43). Each coverslip was only subjected to a single pharmacological treatment. All experiments concluded with high K^+ depolarization to confirm neuronal phenotype and viability, although astrocytes have been shown to respond to high K^+ stimulation as well (44, 45). In $[Ca^{2+}]_o$ Ø experiments K^+ exposure occurred at the beginning of the protocol. The Ca^{2+} responses during αAR agonist treatment in each blocker were compared to their equivalent vehicle treatment (e.g. NE with SERCA Ø vs. vehicle with SERCA Ø).

Variables measured and analysis.

Fura-2 340/380 nm ratios were analyzed using ImageJ (National Institute of Health, Rockville, MD), OriginPro (OriginLab), and Excel 2016 (Microsoft). ImageJ was used to identify neurons based on their bright field and 380 nm fluorescence intensity, obtain the 340 nm and 380 nm intensity values across time, background correct those values from adjacent non-cellular regions, and convert the values into 340/380 nm ratios. As well, ImageJ was used to measure the area of neurons, from which we derived the diameter of each neuron using the equation $[2*\sqrt{A/\pi} = diameter]$ and assuming neurons were spherical following the pruning of their processes. Neurons were eliminated from the dataset if they did not show a clear $[Ca^{2+}]_i$ elevation in response to high K^+ depolarization or looked unhealthy under bright field DIC microscopy. Of the 1218 neurons identified as healthy via bright field, 22.99% (n=280) were eliminated because they did not show a clear high K^+ depolarization. Neurons with excessive spontaneous Ca^{2+} peak frequency and no stable baseline period which prevented measurements were also eliminated from the baseline data set. OriginPro was used to analyze baseline and peak values of background-corrected 340/380 nm ratio traces.

Three parameters were extracted from K^+ depolarization-dependent $[Ca^{2+}]_i$ traces (Fig. 1A): baseline $[Ca^{2+}]_i$ immediately prior to depolarization, absolute peak height of K^+ depolarization-dependent $[Ca^{2+}]_i$ peaks, and amplitude of the K^+ depolarization-dependent $[Ca^{2+}]_i$ peaks (absolute peak height – baseline). To compare peak K^+ 3 *vs.* peak K^+ 4 (i.e. control *vs.* treatment), baseline, absolute peak height, and peak amplitude were converted into percent change [(Peak K^+ 4 / Peak K^+ 3) * 100] and normalized to its imaging aCSF vehicle [(% change treatment / mean % change of vehicle) * 100].

Baseline $[Ca^{2+}]_i$ was extracted from resting $[Ca^{2+}]_i$ traces and was calculated from the 30 s average of the trace at the end of the 5+ min control and 5 min agonist treatment period (Fig. 1B, A and B respectively). Baseline $[Ca^{2+}]_i$ changes were then converted into percent change [(B / A) * 100] and normalized to its equivalent vehicle [(% change treatment / mean % change of equivalent vehicle) * 100]. Using these normalized data the number of responding neurons (i.e. responders) was determined by the number of neurons whose baseline $[Ca^{2+}]_i$ increased by more than 1 standard deviation above its equivalent vehicle response. Responding neuron data is shown as a percent of the total number of neurons in that treatment group.

Frequency and amplitude of spontaneous $[Ca^{2+}]_i$ events, or peaks, was analyzed and defined as the deviation from baseline equaling at least 5% of that neurons high K^+-induced $[Ca^{2+}]_i$ peak. Frequency was calculated as the number of events per 5 min and plotted as a percent change, i.e., [events in agonist treatment / events in control] normalized to vehicle. Amplitude was calculated as absolute peak height – baseline, and for those neurons with multiple events within the 5 min period, averaged to obtain a single value. Amplitude was subsequently calculated as percent change, e.g. [mean amplitude agonist treatment / mean amplitude control] normalized to vehicle. Neurons that did not exhibit a spontaneous event in either the control or treatment period, or in both, were not included in the final dataset. The data that support the findings of this study are available from the corresponding author upon reasonable request.

Statistical analysis was run with GraphPad Prism 7 (GraphPad Software). Students unpaired *t*-tests compared each treatment group (e.g., PE with GCC Ø) to its' equivalent non-agonist vehicle (e.g., vehicle with GCC Ø). One-way ANOVAs compared the magnitude of response among treatment groups (i.e. VEH, NE, PE, CLON, agonist with blockers). To examine responding neuron data Fisher's exact tests compared each treatment group (i.e. NE with SERCA Ø) to its equivalent non-agonist vehicle (i.e. vehicle with SERCA Ø). All tests were run with Fisher's LSD post-hoc test, and a $p < 0.05$ was considered significant. N's denote number of individual cells, from at least 3 rats, in each specific treatment group. Data is shown as individual cells and group means ± standard error of the mean.

RESULTS

NE increases baseline $[Ca^{2+}]_i$ independent of depolarization-induced $[Ca^{2+}]_i$ peaks via α_1-ARs.

The PVN receives dense catecholaminergic innervation from the brainstem (11–13, 17, 18, 40). These NE fibers course throughout the medial and dorsal parvocellular PVN regions where they enhance synaptic transmission and depolarize PVN neurons (17, 25, 27–29, 40). These NE effects are primarily due to alpha adrenergic receptor (α-AR) activation (25, 27, 28, 30). We sought to examine the influence of α-AR activation on $[Ca^{2+}]_i$ influx due to depolarization using the fluorescent Ca^{2+} indicator fura-2. Cells were repeatedly depolarized with high K^+ solution (K^+, 20 s, 5X) intermittent with 5 min washes of imaging aCSF (see Figure 1A) and the influence of AR activation or vehicle on K^+-induced $[Ca^{2+}]_i$ peaks and their initial baseline was determined. PVN neurons under fura-2 380 nm fluorescence and bright field illumination are shown in Figure 2A & B, respectively.

As seen in the representative $[Ca^{2+}]_i$ traces for aCSF alone, high K^+ elevated $[Ca^{2+}]_i$ which promptly returned to resting level (Fig. 2C, black). When PVN neurons were exposed to the general AR agonist NE (Fig. 2C, red, 100 μM) the intermittent baseline period substantially increased, and the subsequent peak 4 amplitude decreased. PE, a specific α_1-AR agonist (Fig. 2C, blue, 10 μM), mimicked the elevated baseline without affecting peak amplitude. In contrast, the α_2-AR agonist CLON (Fig. 2C, orange, 10 μM) did not alter baseline $[Ca^{2+}]_i$ but decreased peak amplitude.

Changes in baseline, absolute peak height, and peak amplitude (peak height - baseline) between control peak 3 and agonist treatment peak 4 (or their prior baseline) are quantified in Figure 2D–F compared to non-agonist aCSF vehicle (VEH). As shown in Figure 2D, baseline $[Ca^{2+}]_i$ between peaks 3 and 4 was significantly higher during NE and PE *vs.* aCSF vehicle. CLON did not alter baseline $[Ca^{2+}]_i$ compared to aCSF vehicle. Absolute peak height (Fig 2E) was significantly increased by PE compared to non-agonist aCSF vehicle (VEH). Conversely, CLON significantly decreased absolute peak height when compared to aCSF vehicle whereas NE non-significantly decreased absolute peak height ($p = 0.062$). K^+-induced peak amplitude (Fig. 2F) significantly decreased in response to NE and CLON compared to VEH, but PE showed no alteration compared to aCSF vehicle. Together, these data demonstrate NE increases baseline $[Ca^{2+}]_i$ via α_1-AR activation whereas peak amplitude decreases via α_2-AR activation.

NE increases overall baseline $[Ca^{2+}]_i$ via the α_1-AR pathway independent of prior depolarization.

To further investigate the α_1-AR mediated baseline $[Ca^{2+}]_i$ increase, we examined the resting $[Ca^{2+}]_i$ independent of prior depolarization and its decay phase. Specifically, we compared $[Ca^{2+}]_i$ in response to 5 minutes of NE, PE or CLON (i.e., agonist treatment) to its preceding aCSF vehicle (*i.e.* control time period). Non-agonist aCSF vehicle (5 min) served as an additional control, and all comparisons were made to this aCSF vehicle (VEH). The 30 s averages at the end of control and treatment determined the percent change of baseline $[Ca^{2+}]_i$, which was normalized to the equivalent aCSF vehicle. At the end of the protocol, cells were depolarized with K^+ to confirm viability (see Figure 1B). Spontaneous Ca^{2+} peaks were also evaluated and are described in subsequent figures.

Representative traces comparing aCSF vehicle alone, NE, PE, and CLON are shown in Figure 3A. During 5 min of aCSF vehicle (black) overall baseline $[Ca^{2+}]_i$ does not change compared to its preceding control period. Bath application of NE or PE (red and blue respectively) increased baseline $[Ca^{2+}]_i$. As shown in the quantitative data (Fig. 3B), when compared to aCSF vehicle, NE and PE significantly increased baseline $[Ca^{2+}]_i$. CLON (orange) tended to decrease baseline $[Ca^{2+}]_i$ (Fig. 3B) but it did not reach significance ($p = 0.2504$, one-way ANOVA). However, when compared only to VEH this decrease by CLON became evident ($p = 0.004$, unpaired *t*-test). Importantly, these results are comparable to those in Figure 2D, demonstrating α_1-AR activation with PE mimics NE's significant increase in baseline $[Ca^{2+}]_i$.

The α_1-AR mediated increase in baseline $[Ca^{2+}]_i$ is due to internal and external Ca^{2+} sources.

To confirm the increase in baseline $[Ca^{2+}]_i$ by NE and PE was due to α_1-AR activation, cells were exposed to the α_1-AR antagonist Prazosin (PRA, 10 μm) prior to exposure to NE or PE. Baseline $[Ca^{2+}]_i$ is shown as percent change during NE or PE in the presence of PRA versus PRA vehicle alone (*i.e.*, NE + PRA *vs.* PRA alone). As Figure 4A&B shows, in the presence of PRA baseline $[Ca^{2+}]_i$ did not increase with NE and PE, and was significantly reduced compared to NE and PE alone ($p < 0.05$, ANOVA), confirming baseline $[Ca^{2+}]_i$ increases by α_1-AR activation.

The increase in baseline $[Ca^{2+}]_i$ by NE and PE may be derived from one or more sources and pathways. The source of the baseline $[Ca^{2+}]_i$ increase was examined by blocking the sarcoplasmic/endoplasmic reticulum Ca^{2+} ATPase (SERCA Ø; Thapsigargin, 1 μM) to eliminate endoplasmic reticular (ER) intracellular Ca^{2+} stores, removing Ca^{2+} from the superfusate ($[Ca^{2+}]_o$ Ø) to eliminate extracellular Ca^{2+}, and using $CdCl_2$ (GCC Ø, 100 μM) as a general Ca^{2+} channel blocker. Given the similarities of NE and PE to enhance baseline $[Ca^{2+}]_i$, SERCA Ø and $[Ca^{2+}]_o$ Ø trials used NE as the agonist and GCC Ø used PE. As with our PRA analysis, baseline $[Ca^{2+}]_i$ is shown as percent change during NE or PE in the presence of blocker normalized to its equivalent blocker vehicle alone (*e.g.*, NE + SERCA Ø *vs.* SERCA Ø alone).

As quantified in Figure 4A, NE in the presence of SERCA Ø significantly reduced the magnitude of the $[Ca^{2+}]_i$ increase and was not significantly different from SERCA Ø with vehicle. $[Ca^{2+}]_o$ significantly eliminated the $[Ca^{2+}]_i$ increase by NE. Similarly, the PE effect was eliminated by GCC Ø (Fig 4B), mimicking the effect of $[Ca^{2+}]_o$ Ø on NE. Overall these data show that both intracellular ER Ca^{2+} stores and external calcium contribute to the α_1-AR mediated increase in baseline $[Ca^{2+}]_i$.

Next we investigated possible intracellular signaling cascades of the α_1-AR mediated baseline $[Ca^{2+}]_i$ increase. The α_1-AR is a G_q coupled receptor that activates phospholipase C (PLC), which in turn activates either inositol trisphosphate (IP_3) or diacylglycerol (DAG) via PIP_2 (46–48). IP_3 subsequently binds to IP_3 receptors (IP_3R) on the ER to mediate ER Ca^{2+} release, whereas DAG activates protein kinase C (PKC) to modify a wide range of downstream signaling pathways (48, 49). The contribution of these pathways in the magnitude of $[Ca^{2+}]_i$ increase by PE was examined by applying PE in the presence of the PLC blocker U73122 (PLC Ø, 1 μM), the PKC blocker Chelerythrine Chloride (PKC Ø, 1 μM), or the IP_3 receptor blocker Xestospongin C (IP_3R Ø, 1 μM). Blockers applied alone served as each groups vehicle control, and was subsequently compared to the responses in PE with an individual inhibitor. All three blockers alone did not alter resting calcium (data not shown). PE (10 μM) in the presence of an individual blocker reduced the overall magnitude of $[Ca^{2+}]_i$ increase and were not significantly different from their inhibitor alone vehicles (unpaired t-test). Comparing the PE response with and without blockers demonstrated only IP_3R Ø was significantly blunted vs. PE alone (one-way ANOVA, Fig. 4B).

We also examined the proportion of neurons that responded to a given activation. Responders were defined as neurons with a baseline $[Ca^{2+}]_i$ increase equal to or greater than the 1 standard deviation above the equivalent vehicles mean overall baseline response (i.e., threshold). Non-responders were any neurons that did not meet that criterion. Figure 4C shows the percent of neurons that responded above threshold with agonist (color) and with vehicle (hatched bars). As shown, NE induced an increase in $[Ca^{2+}]_i$ in ~40% of all neurons tested (i.e., responders) compared to aCSF vehicle, an effect which was mimicked by PE but not by CLON (Fisher's exact test), and eliminated by PRA treatment. When NE was applied during SERCA Ø and $[Ca^{2+}]_o$ the number of responders was reduced and not different than blocker alone. The number of responders during PE was also sufficiently eliminated during GCC Ø and PLC Ø, with a lesser elimination by PKC Ø, and IP_3 Ø.

AR activation does not affect spontaneous calcium peak frequency or amplitude.

The NE-dependent increase in baseline $[Ca^{2+}]_i$ may be related to, or caused by, the increase in frequency and/or size of spontaneous $[Ca^{2+}]_i$ peaks. Within the nTS α_1-AR agonists induce large rhythmic $[Ca^{2+}]_i$ oscillations (39). To examine the effect of NE on spontaneous $[Ca^{2+}]_i$ peaks, the frequency of peaks and the size of those peaks (amplitude) were measured during the 5 min control and agonist treatment periods. A spontaneous $[Ca^{2+}]_i$ peak was defined as any deviation from baseline that was at least 5% of the K^+-induced $[Ca^{2+}]_i$ peak amplitude evoked at the end of the protocol. Representative traces (see Fig. 3A) show minor influence of AR activation on spontaneous $[Ca^{2+}]_i$ peak activity. Quantitative data in Figure 5A and 5B reinforces this conclusion, as neither NE, PE, or CLON altered spontaneous peak frequency or amplitude, although CLON non-significantly decreased amplitude, consistent with results seen in Figure 2F.

DISCUSSION

In the present study we show that NE elicits an increase in baseline $[Ca^{2+}]_i$ in rat hypothalamic PVN neurons. While α_1-AR activation by phenylephrine (PE) mimicked the baseline increase, and α_1-AR antagonization by prazosin (PRA) eliminated the increase, α_2-AR activation by clonidine (CLON) did not significantly influence baseline $[Ca^{2+}]_i$. α_2-AR activation, but not α_1-AR activation, significantly decreased the amplitude of depolarization-induced Ca^{2+} peaks. These data suggest a receptor-specific influence on internal Ca^{2+} control homeostasis. Several pathways play a role in the α-AR elevation of baseline $[Ca^{2+}]_i$, as evidenced by reduction or elimination of Ca^{2+} increases by removal of extracellular Ca^{2+} and blockade of intracellular pathways, including inhibition of PLC, PKC, SERCA, and block of the IP_3R. These data suggest adrenergic receptors elevate intracellular calcium via a multifaceted-signaling complex that may ultimately alter PVN activity and thus its influence on cardiorespiratory and other functions. This cascade, as described above, is presented in Figure 6 and represents our working model.

The PVN contains parvocellular and magnocellular neurons, as well as glutamatergic interneurons (25, 50–52). We isolated neurons within the boundary of the medial magnocellular subneucleus and the 3rd ventricle, an area rich in parvocellular neuroendocrine and autonomic neurons (13). A limitation of the present work is that we did not identify the precise identity of all of the cells examined, including ruling out inclusion of pituitary-projecting magnocellular neurons. While we passed our cultures through a 40 μm filter in the isolation process, neurons in the magnocellular region of the PVN have a diameter up to ~21 μm - smaller than the filter size – and thus unlikely to be completely filtered out (53). Across all of the neurons analyzed in the present study (n = 938), assuming a spherical neuron following pruning of their processes (see figure 2), the average diameter of our neurons was 13.2 ± 0.08 μm (range = 6.2 μm - 27.1 μm), consistent with previous calculations (53); neuronal size did not differ among protocols (data not shown, one-way ANOVA). Thus, the neurons studied likely represent the heterogenous nature of the PVN.

Regardless of the cultured cells phenotype, NE and PE increased baseline $[Ca^{2+}]_i$ in 41.41% and 35.35% (Fig. 4C), respectively, of our cells. The magnitude of response in those neurons was 19.38% and 17.25% over its resting level. When PRA, an α_1-AR antagonist, was

applied prior to NE or PE it eliminated the baseline $[Ca^{2+}]_i$ increase, confirming the critical role of α_1-ARs in this response. Previous studies in PVN slices demonstrate NE has direct effects on PVN neurons, with NE depolarizing 20% of magnocellular neurons (25), and 2% of parvocellular neurons (28). NE also hyperpolarizes 14% of parvocellular neurons via activation of beta receptors (28). While the proportion of responders and the magnitude of their response to α_1-AR activation in our study was greater than others (25, 28), this may be due to differences in techniques. In our isolated cells there is little influence of nearby factors including other neurons or glia present in slices. It is unclear whether the increase in $[Ca^{2+}]_i$ we observe induces or is induced by alterations in neuronal membrane potential. For instance, elevated Ca^{2+} may induce depolarization, as well as activate Ca^{2+}-activated potassium channels to hyperpolarize the cells. Alternatively, the increase in Ca^{2+} may facilitate neuropeptide release, especially within a more intact system. Future studies utilizing simultaneous patch-clamping and fura-2 imaging of PVN neurons will be required to further elucidate this connection. Moreover, whether NE or PE modulate astrocytic calcium to influence neuronal activity perhaps via gliotransmitter release requires further study.

Several sources or pathways may be responsible for the baseline $[Ca^{2+}]_i$ elevations, and the two primary sources that we studied, extracellular Ca^{2+} via plasma membrane proteins and intracellular Ca^{2+} via release from the endoplasmic reticulum, are highlighted in Figure 6. The elimination of $[Ca^{2+}]_i$ elevation by removing extracellular Ca^{2+}, or blocking channels with Cd^{2+} strongly indicates the involvement of one or more plasma membrane proteins. Both magno- and parvocellular neurons express L-type Ca^{2+} channels, and parvocellular neurons express T-type Ca^{2+} channels as well (29, 54, 55). Non-neurosecretory parvocellular neurons have much larger T-type Ca^{2+} currents then neurosecretory parvocellular neurons (51), and these low threshold channels may be responsible for the $[Ca^{2+}]_i$ increase we observe. As our cultures likely contain multiple types of PVN neurons, the differential expression of T-type currents may also explain why only a subset of neurons increased $[Ca^{2+}]_i$ when exposed to NE or PE. In addition, Ca^{2+} permeable transient receptor potential cation (TRP) channels (55) and NMDA receptors (56) are also present in the PVN, and may contribute to $[Ca^{2+}]_i$ influx upon depolarization or phosphorylation. While Cd^{2+} is a prototypical voltage dependent Ca^{2+} channel (VDCC) blocker (57, 58), it has also been shown to block TRP channels (59–61). The persistent decrease in fura-2 fluorescence and number of responders of PE with Cd^{2+} may be due to the persistence of Cd^{2+} inhibition. It does seem clear, however, that L-type and other high-threshold VDCCs are not directly affected by α_1-AR activation because the elevation of $[Ca^{2+}]_i$ by high K^+ depolarization was unmodified by NE or PE.

Our data suggests the NE enhancement of $[Ca^{2+}]_i$ is due to α_1-AR activation because PE, a specific α_1-AR agonist, mimics NE's effect on the magnitude of response, as well as the number of responders, and antagonization of α_1-ARs using PRA eliminated the baseline increase during exposure to NE or PE. The increase in $[Ca^{2+}]_i$ was observed both in cells at rest and following high K^+ induced depolarization. The observation of the former suggested the Ca^{2+} rise is not due to slowing of high K^+ response. Our conclusion is consistent with other work on the excitatory influence of α_1-ARs in the PVN (25, 27, 28, 62), in particular showing NE increased action potential (AP) discharge in the PVN by an α_1-AR mediated

direct membrane depolarization as well as an increase in excitatory post-synaptic potentials (EPSPs). While an increase in glutamatergic synaptic currents may activate Ca^{2+}-permeable glutamate receptors, including NMDA receptors, our data suggests the α_1-AR may have direct influence on PVN neurons. The supraoptic nucleus (SON), a similar hypothalamic nucleus innervated by adrenergic projections from the nTS and VLM (17, 40), has similar α_1-AR mediated excitation. Specifically, NE increased SON excitability via an α_1-AR mediated increase in burst firing, and α_1-AR activation also increases $[Ca^{2+}]_i$ in the SON (35–38) similar to results seen in the PVN. However, NE has also been observed to decrease excitability in the SON as well (63–65). In the nTS, an important cardiorespiratory nucleus that contains PVN projecting adrenergic neurons (8), α_1-AR activation stimulates $[Ca^{2+}]_i$ influx, although as oscillations and not the consistent increase we see in PVN neurons (39). In other central neurons, α_1-AR activation increases AP discharge and depolarizes membranes in the rat medial pontine reticular formation (66), excites mouse purkinje neurons (67), induces Ca^{2+} oscillations in the anterior pituitary (52), as well as increases EPSP frequency and induces membrane depolarization in the rat sacral autonomic nucleus (68). The α_1-AR mediated $[Ca^{2+}]_i$ increase we observe fits closely with these other studies. Further experiments are needed to confirm the relationship between the α_1-AR mediated $[Ca^{2+}]_i$ increase we observe and α_1-AR mediated increased excitability observed by others.

NE and PE binding of α_1-AR activates G_q and thus several second messenger pathways including; the classical PLC to IP_3 or DAG via PIP_2, where DAG activates PKC and IP_3 activates ER Ca^{2+} stores (47, 48, 69, 70), seen in Figure 6; cAMP to PKA (37); and even $cPLA_2$ activation (70). We inhibited several parts of the classical α_1 second messenger pathway and found that while blocking PLC and PKC attenuated PE's effect, they did not completely abolish the $[Ca^{2+}]_i$ increase (a ~ 7–10 % increase with PE remained). Only IP_3R block significantly eliminated the PE response. While this suggests PLC, PKC, and IP_3R play a role in the α_1-AR mediated $[Ca^{2+}]_i$ increase, we cannot rule out other, non-traditional pathways play a role. Studies have shown that α_1-AR activation can trigger cAMP and PKA signaling (37), $cPLA_2$ (70), and even ERK pathway acitvation (46, 71). These signaling pathways, especially the ones involving PKC and PKA, may phosphorylate Ca^{2+} channels and modify their behavior (41), including lowering the activation threshold for T-type Ca^{2+} channels (72) or increasing the L-type Ca^{2+} current (73, 74). Phosphorylation of TRP channels, such as those TRPV channels found throughout the PVN, enhances Ca^{2+} current (75–77). In addition to the elimination of the NE and PE responses by removing or blocking extracellular sources, SERCA block was used to empty ER Ca^{2+} stores and eliminate their influence, and it attenuated but did not completely eliminate the $[Ca^{2+}]_i$ increase by NE. This suggests that extracellular Ca^{2+} is the primary source of $[Ca^{2+}]_i$ and that ER stores play either a secondary role or are triggered by extracellular Ca^{2+} influx. This may be through Ca^{2+}-induced Ca^{2+}-release mechanisms, where Ca^{2+} influx into the cytosol stimulates ER Ca^{2+} stores to release Ca^{2+} into the cytosol (49). Alternatively the attenuation but incomplete elimination of the $[Ca^{2+}]_i$ increase after SERCA block could be the result of Ca^{2+} release-activated Ca^{2+}, where ER depletion stimulates extracellular Ca^{2+} influx through store operated Ca^{2+} channels (42, 78). In this case the Ca^{2+} increase would be unrelated to adrenergic stimulation and would instead be the direct result of SERCA block, however, the $[Ca^{2+}]_i$ increase during NE exposure is not mimicked in SERCA block vehicle,

suggesting NE, and not ER depletion and subsequent Ca^{2+} release-activated Ca^{2+}, is responsible. IP_3R activation can be enhanced by $[Ca^{2+}]_i$ (79–84) which can create a synergistic relationship were extracellular influx or ER release alone account for a small $[Ca^{2+}]_i$ change, but when they occur together there is a large $[Ca^{2+}]_i$ increase (82). Thus, unlinking this process via either removal of extracellular or ER sources may limit NE influence on $[Ca^{2+}]_i$. Here, however, the total abolishment of the affect when extracellular Ca^{2+} is removed suggests that extracellular Ca^{2+} influx is a primary event, with ER Ca^{2+} stores also contributing to the full effect.

NE's effects were not confined to the α_1-AR mediated increase in baseline $[Ca^{2+}]_i$, we also observed a decrease in voltage-activated (high K^+) Ca^{2+} influx that was mimicked by α_2-AR activation (Fig. 6). Cummings and Seybold (19) have demonstrated the presence of both α_1 and α_2 ARs in the PVN, and α_2-ARs have been shown to have inhibitory effects in PVN parvocellular neurons (27, 28, 85). In mouse PVN neurons α_2-AR activation inhibited 59% of treated cells, while α_1 and β-ARs excited 35% of treated cells (85). In several other regions that express inhibitory α_2-ARs, such as Purkinje neurons in the cerebellum (67), and in the sacral autonomic nucleus (68), α_2 activation leads to an increase in outward current and decrease in EPSP frequency. NE has also been shown to decrease excitability in the SON, a related hypothalamic nucleus (63–65). This suggests that α_2 activation modified the behavior of VDCCs, possibly through high-threshold, Ca^{2+} channels, but future studies are needed to examine the pathway of α_2-AR inhibition.

In contrast to the NE and PE increase in baseline $[Ca^{2+}]$i and CLON decrease in K+ depolarization-induced $[Ca^{2+}]$, we did not see a robust influence of α_1 or α_2 receptors on spontaneous events. This is in contrast with work done in the nTS (39). We classified spontaneous events to be any $[Ca^{2+}]_i$ increases that were equal to or greater than 5% of that cells high K^+ $[Ca^{2+}]_i$ response. It could be that this 5% cut off was either too small and did not filter out the noise, or was too large and eliminated our effect, however even when our threshold was changed to as small as 1% or as large as 20% NE and CLON did not alter spontaneous events (data not shown, paired t-test).

Hypoxia activates PVN-projecting adrenergic neurons, particularly those in the nTS (8, 10), and NE increases PVN excitation (1, 2, 4, 86–88). PVN over-activity, including that caused by long-term hypoxic exposure such as with obstructive sleep apnea (7), correlates with negative health outcomes such as hypertension, heart failure, and stroke (6, 87). Within the PVN hypoxia increases FOS expression in many PVN neurons, including CRH expressing neurons that are within the area that we isolated (2, 89), and NE has been directly linked to increased plasma levels and production of CRH (90), possibly due to α_1-AR activation. The PVN also plays an important role in regulating feeding behavior, as well as glucose and insulin levels in the blood (91). Catecholaminergic projections from the hindbrain to the PVN, especially norandrenergic projections, play an important role in regulating those behaviors (17, 92, 93). PVN stimulation by NE has been shown to increase blood glucose levels and suppress insulin levels (94), and prompt a consistent feeding response in rats (95). Watts *et. al.* demonstrated that NE activated an ERK1/2 pathway in CRH neuroendocrine neurons, and that this pathway was activated by hindbrain sensation of glycaemia related stressors (96). The effects of NE on PVN neurons observed in this study could be related to

either of these two functions, or others, and future experiments are needed to investigate the specific neuronal phenotype and what, if any, role the $[Ca^{2+}]_i$ increase we observe may play in them.

In summary, we have demonstrated that NE increases $[Ca^{2+}]_i$ levels in PVN neurons independent of depolarization-induced Ca^{2+} influx or changes in spontaneous Ca^{2+} event frequency or amplitude. We suggest this increase is mediated by α_1-AR activation, and is co-dependent on extracellular Ca^{2+} influx, most likely through one or more calcium channels, and Ca^{2+} release from intracellular stores, which supports pervious work showing NE induces increased discharge and membrane depolarization via the α_1-AR (25, 27–29). Given previous work showing NE is released in the PVN by various catecholaminergic neurons projecting from surrounding nuclei, these data contribute to a better understanding of NE's role in affecting PVN behavior.

Acknowledgements:

Funded by RO1 HL098602 (DDK)

References

1. Coldren KM, Li D-P, Kline DD, Hasser EM, Heesch CM. Acute hypoxia activates neuroendocrine, but not presympathetic, neurons in the paraventricular nucleus of the hypothalamus: differential role of nitric oxide. American Journal of Physiology-Regulatory, Integrative and Comparative Physiology. 2017; 312(6): R982–R95.
2. Ruyle BC, Klutho PJ, Baines CP, Heesch CM, Hasser EM. Hypoxia activates a neuropeptidergic pathway from the paraventricular nucleus of the hypothalamus to the nucleus tractus solitarii. Am J Physiol Regul Integr Comp Physiol. 2018; 315(6): R1167–R82. [PubMed: 30230933]
3. Smith DW, Buller KM, Day TA. Role of ventrolateral medulla catecholamine cells in hypothalamic neuroendocrine cell responses to systemic hypoxia. The Journal of Neuroscience. 1995; 15(12): 7979. [PubMed: 8613735]
4. Knight WD, Little JT, Carreno FR, Toney GM, Mifflin SW, Cunningham JT. Chronic intermittent hypoxia increases blood pressure and expression of FosB/ΔFosB in central autonomic regions. American Journal of Physiology-Regulatory, Integrative and Comparative Physiology. 2011; 301(1): R131–R9.
5. Olivan MV, Bonagamba LGH, Machado BH. Involvement of the paraventricular nucleus of the hypothalamus in the pressor response to chemoreflex activation in awake rats. Brain Research. 2001; 895(1): 167–72. [PubMed: 11259774]
6. Sharpe AL, Calderon AS, Andrade MA, Cunningham JT, Mifflin SW, Toney GM. Chronic intermittent hypoxia increases sympathetic control of blood pressure: role of neuronal activity in the hypothalamic paraventricular nucleus. American Journal of Physiology-Heart and Circulatory Physiology. 2013; 305(12): H1772–H80. [PubMed: 24097432]
7. Kc P, Dick TE. Modulation of cardiorespiratory function mediated by the paraventricular nucleus. Respiratory physiology & neurobiology. 2010; 174(1–2): 55–64. [PubMed: 20708107]
8. King TL, Heesch CM, Clark CG, Kline DD, Hasser EM. Hypoxia activates nucleus tractus solitarii neurons projecting to the paraventricular nucleus of the hypothalamus. American Journal of Physiology-Regulatory, Integrative and Comparative Physiology. 2012; 302(10): R1219–R32.
9. Hirooka Y, Polson JW, Potts PD, Dampney RAL. Hypoxia-induced Fos expression in neurons projecting to the pressor region in the rostral ventrolateral medulla. Neuroscience. 1997; 80(4): 1209–24. [PubMed: 9284071]
10. King TL, Kline DD, Ruyle BC, Heesch CM, Hasser EM. Acute systemic hypoxia activates hypothalamic paraventricular nucleus-projecting catecholaminergic neurons in the caudal

ventrolateral medulla. American Journal of Physiology-Regulatory, Integrative and Comparative Physiology. 2013; 305(10): R1112–R23.

11. Cunningham ET, Sawchenko PE. Anatomical specificity of noradrenergic inputs to the paraventricular and supraoptic nuclei of the rat hypothalamus. Journal of Comparative Neurology. 1988; 274(1): 60–76. [PubMed: 2458397]
12. Cunningham ET, Bohn MC, Sawchenko PE. Organization of adrenergic inputs to the paraventricular and supraoptic nuclei of the hypothalamus in the rat. Journal of Comparative Neurology. 1990; 292(4): 651–67. [PubMed: 2324319]
13. Swanson LW, Sawchenko PE. Paraventricular Nucleus: A Site for the Integration of Neuroendocrine and Autonomic Mechanisms. Neuroendocrinology. 1980; 31(6): 410–7. [PubMed: 6109264]
14. Mc Neill TH, Sladek JR Jr. Simultaneous monoamine histofluorescence and neuropeptide immunocytochemistry: II. Correlative distribution of catecholamine varicosities and magnocellular neurosecretory neurons in the rat supraoptic and paraventricular nuclei. Journal of Comparative Neurology. 1980; 193(4): 1023–33. [PubMed: 7000861]
15. Bienkowski MS, Rinaman L. Noradrenergic inputs to the paraventricular hypothalamus contribute to hypothalamic–pituitary–adrenal axis and central Fos activation in rats after acute systemic endotoxin exposure. Neuroscience. 2008; 156(4): 1093–102. [PubMed: 18773942]
16. Chen XQ, Du JZ, Wang YS. Regulation of hypoxia-induced release of corticotropin-releasing factor in the rat hypothalamus by norepinephrine. Regul Pept. 2004; 119(3): 221–8. [PubMed: 15120484]
17. Sawchenko PE, Swanson LW. Central noradrenergic pathways for the integration of hypothalamic neuroendocrine and autonomic responses. Science. 1981; 214(4521): 685. [PubMed: 7292008]
18. Swanson LW, Sawchenko PE, Bérod A, Hartman BK, Helle KB, Vanorden DE. An immunohistochemical study of the organization of catecholaminergic cells and terminal fields in the paraventricular and supraoptic nuclei of the hypothalamus. Journal of Comparative Neurology. 1981; 196(2): 271–85. [PubMed: 6111572]
19. Cummings S, Seybold V. Relationship of Alpha-1- and Alpha-2-Adrenergic-Binding Sites to Regions of the Paraventricular Nucleus of the Hypothalamus Containing Corticotropin-Releasing Factor and Vasopressin Neurons. Neuroendocrinology. 1988; 47(6): 523–32. [PubMed: 2899848]
20. Calogero AE, Gallucci WT, Chrousos GP, Gold PW. Catecholamine effects upon rat hypothalamic corticotropin-releasing hormone secretion in vitro. The Journal of clinical investigation. 1988; 82(3): 839–46. [PubMed: 2901433]
21. Day HEW, Campeau S, Watson SJ, Akil H. Distribution of α1a-, α1b- and α1d-adrenergic receptor mRNA in the rat brain and spinal cord. Journal of Chemical Neuroanatomy. 1997; 13(2): 115–39. [PubMed: 9285356]
22. Nicholas AP, Pieribone V, Hökfelt T. Distributions of mRNAs for alpha-2 adrenergic receptor subtypes in rat brain: An in situ hybridization study. Journal of Comparative Neurology. 1993; 328(4): 575–94. [PubMed: 8381444]
23. Scheinin M, Lomasney JW, Hayden-Hixson DM, Schambra UB, Caron MG, Lefkowitz RJ, Fremeau RT. Distribution of α2-adrenergic receptor subtype gene expression in rat brain. Molecular Brain Research. 1994; 21(1): 133–49. [PubMed: 8164514]
24. Nicholas AP, Pieribone VA, Hökfelt T. Cellular localization of messenger RNA for beta-1 and beta-2 adrenergic receptors in rat brain: An in situ hybridization study. Neuroscience. 1993; 56(4): 1023–39. [PubMed: 8284033]
25. Daftary SS, Boudaba C, Szabó K, Tasker JG. Noradrenergic Excitation of Magnocellular Neurons in the Rat Hypothalamic Paraventricular Nucleus via Intranuclear Glutamatergic Circuits. The Journal of Neuroscience. 1998; 18(24): 10619. [PubMed: 9852597]
26. Boudaba C, Di S, Tasker JG. Presynaptic Noradrenergic Regulation of Glutamate Inputs to Hypothalamic Magnocellular Neurones. Journal of Neuroendocrinology. 2003; 15(8): 803–10. [PubMed: 12834442]
27. Yang JH, Li LH, Lee S, Jo IH, Lee SY, Ryu PD. Effects of Adrenalectomy on the Excitability of Neurosecretory Parvocellular Neurones in the Hypothalamic Paraventricular Nucleus. Journal of Neuroendocrinology. 2007; 19(4): 293–301. [PubMed: 17355319]

28. Daftary SS, Boudaba C, Tasker JG. Noradrenergic regulation of parvocellular neurons in the rat hypothalamic paraventricular nucleus. Neuroscience. 2000; 96(4): 743–51. [PubMed: 10727792]
29. Luther JA, Tasker JG. Voltage-gated currents distinguish parvocellular from magnocellular neurones in the rat hypothalamic paraventricular nucleus. The Journal of Physiology. 2000; 523(1): 193–209. [PubMed: 10673555]
30. Chen Q, Li D-P, Pan H-L. Presynaptic α1 Adrenergic Receptors Differentially Regulate Synaptic Glutamate and GABA Release to Hypothalamic Presympathetic Neurons. Journal of Pharmacology and Experimental Therapeutics. 2006; 316(2): 733. [PubMed: 16249372]
31. Vacher C-M, Frétier P, Créminon C, Calas A, Hardin-Pouzet H. Activation by Serotonin and Noradrenaline of Vasopressin and Oxytocin Expression in the Mouse Paraventricular and Supraoptic Nuclei. The Journal of Neuroscience. 2002; 22(5): 1513. [PubMed: 11880481]
32. Bridges TE, Hillhouse EW, Jones MT. The effect of dopamine on neurohypophysial hormone release in vivo and from the rat neural lobe and hypothalamus in vitro. The Journal of Physiology. 1976; 260(3): 647–66. [PubMed: 988183]
33. Leibowitz SF, Eidelman D, Suh JS, Diaz S, Sladek CD. Mapping study of noradrenergic stimulation of vasopressin release. Experimental Neurology. 1990; 110(3): 298–305. [PubMed: 2249740]
34. Benetos A, Gavras I, Gavras H. Norepinephrine applied in the paraventricular hypothalamic nucleus stimulates vasopressin release. Brain Research. 1986; 381(2): 322–6. [PubMed: 3827993]
35. Randle JCR, Bourque CW, Renaud LP. α-Adrenergic activation of rat hypothalamic supraoptic neurons maintained in vitro. Brain Research. 1984; 307(1): 374–8. [PubMed: 6087990]
36. Randle JC, Bourque CW, Renaud LP. Alpha 1-adrenergic receptor activation depolarizes rat supraoptic neurosecretory neurons in vitro. American Journal of Physiology-Regulatory, Integrative and Comparative Physiology. 1986; 251(3): R569–R74.
37. Shioda S, Yada T, Muroya S, Takigawa M, Nakai Y. Noradrenaline activates vasopressin neurons via α1-receptor-mediated Ca2+ signaling pathway. Neuroscience Letters. 1997; 226(3): 210–2. [PubMed: 9175604]
38. Song Z, Gomes DA, Stevens W, Sladek CD. Multiple α1-adrenergic receptor subtypes support synergistic stimulation of vasopressin and oxytocin release by ATP and phenylephrine. American Journal of Physiology-Regulatory, Integrative and Comparative Physiology. 2010; 299(6): R1529–R37.
39. Hermann GE, Nasse JS, Rogers RC. α−1 adrenergic input to solitary nucleus neurones: calcium oscillations, excitation and gastric reflex control. J Physiol. 2005; 562(2): 553–68. [PubMed: 15539398]
40. Sawchenko PE, Swanson LW. The organization of noradrenergic pathways from the brainstem to the paraventricular and supraoptic nuclei in the rat. Brain Research Reviews. 1982; 4(3): 275–325.
41. Catterall WA. Voltage-gated calcium channels. Cold Spring Harbor perspectives in biology. 2011; 3(8): a003947–a. [PubMed: 21746798]
42. Ostrowski TD, Dantzler HA, Polo-Parada L, Kline DD. H2O2 augments cytosolic calcium in nucleus tractus solitarii neurons via multiple voltage-gated calcium channels. Am J Phyiol Cell Physiol. 2017; 312(5): C651–C62.
43. Gafni J, Munsch JA, Lam TH, Catlin MC, Costa LG, Molinski TF, Pessah IN. Xestospongins: Potent Membrane Permeable Blockers of the Inositol 1,4,5-Trisphosphate Receptor. Neuron. 1997; 19(3): 723–33. [PubMed: 9331361]
44. Song Y, Gunnarson E. Potassium dependent regulation of astrocyte water permeability is mediated by cAMP signaling. PLoS One. 2012; 7(4): e34936–e. [PubMed: 22493723]
45. Duffy S, MacVicar BA. Potassium-dependent calcium influx in acutely isolated hippocampal astrocytes. Neuroscience. 1994; 61(1): 51–61. [PubMed: 7969895]
46. Marshall I, Burt RP, Chapple CR. Signal Transduction Pathways Associated with α1-Adrenoceptor Subtypes in Cells and Tissues Including Human Prostate. European Urology. 1999; 36(suppl 1) (Suppl. 1): 42–7. [PubMed: 10393472]
47. Kapoor JR, Sladek CD. Purinergic and Adrenergic Agonists Synergize in Stimulating Vasopressin and Oxytocin Release. The Journal of Neuroscience. 2000; 20(23): 8868. [PubMed: 11102496]

48. Chen Z-j, Minneman KP Recent progress in α1-adrenergic receptor research. Acta Pharmacologica Sinica. 2005; 261281.
49. Berridge MJ. Neuronal Calcium Signaling. Neuron. 1998; 21(1): 13–26. [PubMed: 9697848]
50. Ferguson AV, Latchford KJ, Samson WK. The paraventricular nucleus of the hypothalamus - a potential target for integrative treatment of autonomic dysfunction. Expert opinion on therapeutic targets. 2008; 12(6): 717–27. [PubMed: 18479218]
51. Luther JA, Daftary SS, Boudaba C, Gould GC, Halmos KC, Tasker JG. Neurosecretory and Non-Neurosecretory Parvocellular Neurones of the Hypothalamic Paraventricular Nucleus Express Distinct Electrophysiological Properties. Journal of Neuroendocrinology. 2002; 14(12): 929–32. [PubMed: 12472873]
52. Tse A, Tse FW. alpha-adrenergic stimulation of cytosolic Ca2+ oscillations and exocytosis in identified rat corticotrophs. The Journal of physiology. 1998; 512 (Pt 2)(Pt 2): 385–93. [PubMed: 9763629]
53. Kiss JZ, Martos J, Palkovits M. Hypothalamic paraventricular nucleus: A quantitative analysis of cytoarchitectonic subdivisions in the rat. Journal of Comparative Neurology. 1991; 313(4): 563–73. [PubMed: 1783681]
54. Lee S, Han TH, Sonner PM, Stern JE, Ryu PD, Lee SY. Molecular characterization of T-type Ca2+ channels responsible for low threshold spikes in hypothalamic paraventricular nucleus neurons. Neuroscience. 2008; 155(4): 1195–203. [PubMed: 18657597]
55. Feetham CH, O'Brien F, Barrett-Jolley R. Ion Channels in the Paraventricular Hypothalamic Nucleus (PVN); Emerging Diversity and Functional Roles. Frontiers in Physiology. 2018; 9(760).
56. Qiao X, Zhou J-J, Li D-P, Pan H-L. Src Kinases Regulate Glutamatergic Input to Hypothalamic Presympathetic Neurons and Sympathetic Outflow in Hypertension. Hypertension. 2017; 69(1): 154–62. [PubMed: 27802416]
57. Thévenod F, Jones SW. Cadmium block of calcium current in frog sympathetic neurons. Biophysical Journal. 1992; 63(1): 162–8. [PubMed: 1330026]
58. Lansman JB, Hess P, Tsien RW. Blockade of current through single calcium channels by Cd2+, Mg2+, and Ca2+. Voltage and concentration dependence of calcium entry into the pore. The Journal of General Physiology. 1986; 88(3): 321. [PubMed: 2428920]
59. Pelucchi B, Aguiari G, Pignatelli A, Manzati E, Witzgall R, del Senno L, Belluzzi O. Nonspecific Cation Current Associated with Native Polycystin-2 in HEK-293 Cells. Journal of the American Society of Nephrology. 2006; 17(2): 388. [PubMed: 16396967]
60. Andersson DA, Gentry C, Moss S, Bevan S. Clioquinol and pyrithione activate TRPA1 by increasing intracellular Zn2+. Proceedings of the National Academy of Sciences. 2009; 106(20): 8374.
61. Miura S, Takahashi K, Imagawa T, Uchida K, Saito S, Tominaga M, Ohta T. Involvement of TRPA1 activation in acute pain induced by cadmium in mice. Molecular pain. 2013; 97-.
62. Antoni FA. Hypothalamic Control of Adrenocorticotropin Secretion: Advances since the Discovery of 41-Residue Corticotropin-Releasing Factor. Endocrine Reviews. 1986; 7(4): 351–78. [PubMed: 3023041]
63. Arnauld E, Cirino M, Layton BS, Renaud LP. Contrasting Actions of Amino Acids, Acetylcholine, Noradrenaline and Leucine Enkephalin on the Excitability of Supraoptic Vasopressin-Secreting Neurons. Neuroendocrinology. 1983; 36(3): 187–96. [PubMed: 6835474]
64. Barker JL, Crayton JW, Nicoll RA. Noradrenaline and acetylcholine responses of supraoptic neurosecretory cells. The Journal of Physiology. 1971; 218(1): 19–32. [PubMed: 4399777]
65. Sladek CD, Yagil G. Diverse Effects of Norepinephrine on Vasopressin Release may Reflect Modulation by Hypotonicity. Journal of Neuroendocrinology. 1990; 2(3): 363–7. [PubMed: 19215361]
66. Stevens DR, McCarley RW, Greene RW. The mechanism of noradrenergic alpha 1 excitatory modulation of pontine reticular formation neurons. The Journal of Neuroscience. 1994; 14(11): 6481. [PubMed: 7965052]
67. Hirono M, Obata K. α-Adrenoceptive Dual Modulation of Inhibitory GABAergic Inputs to Purkinje Cells in the Mouse Cerebellum. Journal of Neurophysiology. 2006; 95(2): 700–8. [PubMed: 16251261]

68. Kawatani M, Akimoto N, Yamada A, Furue H, Kawatani M. Noradrenergic effects in rat sacral autonomic nucleus using in vitro slice patch-clamp. Biomedical Research. 2017; 38(6): 359–69. [PubMed: 29225214]
69. Kim JH, Shin SY, Nam JH, Hong E-K, Chung Y-S, Jeong JY, Kang J, Uhm D-Y, Kim SJ. Adrenergic regulation of the intracellular [Ca2+] and voltage-operated Ca2+ channel currents in the rat prostate neuroendocrine cells. The Prostate. 2003; 57(2): 99–110. [PubMed: 12949933]
70. Kreda SM, Sumner M, Fillo S, Ribeiro CM, Luo GX, Xie W, Daniel KW, Shears S, Collins S, Wetsel WC. α1-Adrenergic Receptors Mediate LH-Releasing Hormone Secretion through Phospholipases C and A2 in Immortalized Hypothalamic Neurons. Endocrinology. 2001; 142(11): 4839–51. [PubMed: 11606452]
71. Kong F, Ma L, Zou L, Meng K, Ji T, Zhang L, Zhang R, Jiao J. Alpha1-Adrenergic Receptor Activation Stimulates Calcium Entry and Proliferation via TRPC6 Channels in Cultured Human Mesangial Cells. Cellular Physiology and Biochemistry. 2015; 36(5): 1928–38. [PubMed: 26202353]
72. Yao J, Davies LA, Howard JD, Adney SK, Welsby PJ, Howell N, Carey RM, Colbran RJ, Barrett PQ. Molecular basis for the modulation of native T-type Ca2+ channels in vivo by Ca2+/calmodulin-dependent protein kinase II. The Journal of Clinical Investigation. 2006; 116(9): 2403–12. [PubMed: 16917542]
73. Yang L, Liu G, Zakharov SI, Morrow JP, Rybin VO, Steinberg SF, Marx SO. Ser1928 Is a Common Site for Cav1.2 Phosphorylation by Protein Kinase C Isoforms. Journal of Biological Chemistry. 2005; 280(1): 207–14. [PubMed: 15509562]
74. Hulme JT, Lin TWC, Westenbroek RE, Scheuer T, Catterall WA. β-Adrenergic regulation requires direct anchoring of PKA to cardiac Ca_V 1.2 channels via a leucine zipper interaction with A kinase-anchoring protein 15. Proceedings of the National Academy of Sciences. 2003; 100(22): 13093.
75. Yao X, Kwan HY, Huang Y. Regulation of TRP Channels by Phosphorylation. Neurosignals. 2005; 14(6): 273–80. [PubMed: 16772730]
76. Xu F, Satoh E, Iijima T. Protein kinase C-mediated Ca2+ entry in HEK 293 cells transiently expressing human TRPV4. British journal of pharmacology. 2003; 140(2): 413–21. [PubMed: 12970074]
77. Numazaki M, Tominaga T, Toyooka H, Tominaga M. Direct Phosphorylation of Capsaicin Receptor VR1 by Protein Kinase Cε and Identification of Two Target Serine Residues. Journal of Biological Chemistry. 2002; 277(16): 13375–8. [PubMed: 11884385]
78. Hoth M, Penner R. Depletion of intracellular calcium stores activates a calcium current in mast cells. Nature. 1992; 355(6358): 353–6. [PubMed: 1309940]
79. Padamsey Z, Foster WJ, Emptage NJ. Intracellular Ca2+ Release and Synaptic Plasticity: A Tale of Many Stores. The Neuroscientist. 20181073858418785334.
80. Nakamura T, Nakamura K, Lasser-Ross N, Barbara J-G, Sandler VM, Ross WN. Inositol 1,4,5-Trisphosphate (IP_3)-Mediated Ca2+ Release Evoked by Metabotropic Agonists and Backpropagating Action Potentials in Hippocampal CA1 Pyramidal Neurons. The Journal of Neuroscience. 2000; 20(22): 8365. [PubMed: 11069943]
81. Nakamura T, Lasser-Ross N, Nakamura K, Ross WN. Spatial segregation and interaction of calcium signalling mechanisms in rat hippocampal CA1 pyramidal neurons. The Journal of physiology. 2002; 543(Pt 2): 465–80. [PubMed: 12205182]
82. Nakamura T, Barbara J-G, Nakamura K, Ross WN. Synergistic Release of Ca2+ from IP3-Sensitive Stores Evoked by Synaptic Activation of mGluRs Paired with Backpropagating Action Potentials. Neuron. 1999; 24(3): 727–37. [PubMed: 10595522]
83. Stutzmann GE, LaFerla FM, Parker I. Calcium Signaling in Mouse Cortical Neurons Studied by Two-Photon Imaging and Photoreleased Inositol Triphosphate. The Journal of Neuroscience. 2003; 23(3): 758. [PubMed: 12574404]
84. Taylor CW, Tovey SC. IP(3) receptors: toward understanding their activation. Cold Spring Harbor perspectives in biology. 2010; 2(12): a004010–a. [PubMed: 20980441]

85. Inenaga K, Dyball REJ, Okuya S, Yamashita H. Characterization of hypothalamic noradrenaline receptors in the supraoptic nucleus and periventricular region of the paraventricular nucleus of mice in vitro. Brain Research. 1986; 369(1): 37–47. [PubMed: 3008940]

86. Dillon GH, Waldrop TG. In vitro responses of caudal hypothalamic neurons to hypoxia and hypercapnia. Neuroscience. 1992; 51(4): 941–50. [PubMed: 1336828]

87. Shell B, Faulk K, Cunningham JT. Neural Control of Blood Pressure in Chronic Intermittent Hypoxia. Current Hypertension Reports. 2016; 18(3): 19. [PubMed: 26838032]

88. Berquin P, Bodineau L, Gros F, Larnicol N. Brainstem and hypothalamic areas involved in respiratory chemoreflexes: a Fos study in adult rats. Brain Research. 2000; 857(1): 30–40. [PubMed: 10700550]

89. Maruyama NO, Mitchell NC, Truong TT, Toney GM. Activation of the hypothalamic paraventricular nucleus by acute intermittent hypoxia: Implications for sympathetic long-term facilitation neuroplasticity. Experimental Neurology. 2019; 3141–8.

90. Itoi K, Suda T, Tozawa F, Dobashi I, Ohmori N, Sakai Y, Abe K, Demura H. Microinjection of norepinephrine into the paraventricular nucleus of the hypothalamus stimulates corticotropin-releasing factor gene expression in conscious rats. Endocrinology. 1994; 135(5): 2177–82. [PubMed: 7956940]

91. Steffens AB, Scheurink AJW, Luiten PGM, Bohus B. Hypothalamic food intake regulating areas are involved in the homeostasis of blood glucose and plasma FFA levels. Physiology & Behavior. 1988; 44(4): 581–9. [PubMed: 3070585]

92. Ritter S, Watts AG, Dinh TT, Sanchez-Watts G, Pedrow C. Immunotoxin Lesion of Hypothalamically Projecting Norepinephrine and Epinephrine Neurons Differentially Affects Circadian and Stressor-Stimulated Corticosterone Secretion. Endocrinology. 2003; 144(4): 1357–67. [PubMed: 12639919]

93. Ritter S, Llewellyn-Smith I, Dinh TT. Subgroups of hindbrain catecholamine neurons are selectively activated by 2-deoxy-d-glucose induced metabolic challenge. Brain Research. 1998; 805(1): 41–54. [PubMed: 9733914]

94. Ionescu E, Coimbra CC, Walker CD, Jeanrenaud B. Paraventricular nucleus modulation of glycemia and insulinemia in freely moving lean rats. American Journal of Physiology-Regulatory, Integrative and Comparative Physiology. 1989; 257(6): R1370–R6.

95. Leibowitz SF, Sladek C, Spencer L, Tempel D. Neuropeptide Y, epinephrine and norepinephrine in the paraventricular nucleus: Stimulation of feeding and the release of corticosterone, vasopressin and glucose. Brain Research Bulletin. 1988; 21(6): 905–12. [PubMed: 3224284]

96. Khan AM, Kaminski KL, Sanchez-Watts G, Ponzio TA, Kuzmiski JB, Bains JS, Watts AG. MAP Kinases Couple Hindbrain-Derived Catecholamine Signals to Hypothalamic Adrenocortical Control Mechanisms during Glycemia-Related Challenges. The Journal of Neuroscience. 2011; 31(50): 18479. [PubMed: 22171049]

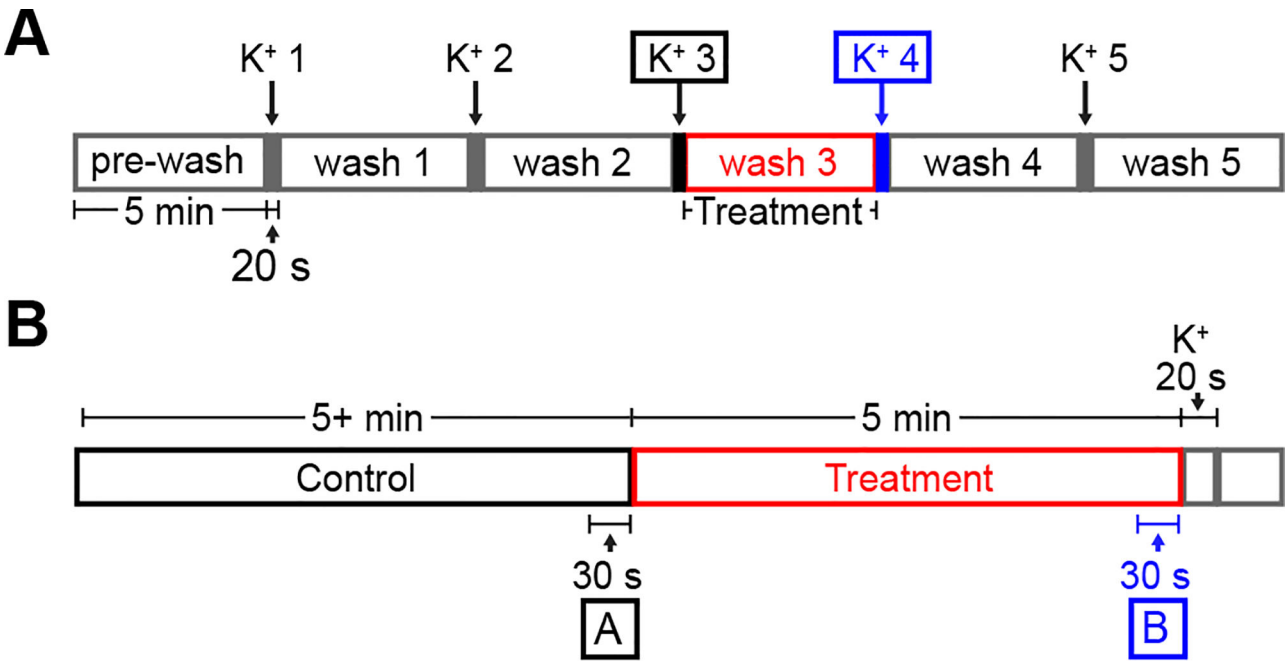

Figure 1. Protocols used to examine the influence of AR activation on depolarization induced $[Ca^{2+}]_i$ and resting $[Ca^{2+}]_i$.

***A*:** Repeated high K^+ (K^+) exposure was used to examine the influence of AR activation on depolarization induced $[Ca^{2+}]_i$. Neurons were depolarized 5 times (20 s each, K^+ 1–5) with washes in between (imaging aCSF, 5 min each, wash 1–5). NE, PE, CLON, or aCSF vehicle was applied during wash 3 (red). The baseline $[Ca^{2+}]_i$ immediately prior to high K^+ depolarization, K^+-induced total peak height, and K^+-induced peak amplitude (i.e., total peak height – baseline) were recorded. ***B*:** To examine the influence of AR activation on resting $[Ca^{2+}]_i$, the control time period (black, 5+ min) was compared to the treatment time period (red, 5 min) using the following measures: the average baseline $[Ca^{2+}]_i$ at A and B, the number of neurons that had a baseline response greater than one standard deviation above the equivalent average vehicle response, and the frequency and amplitude of spontaneous $[Ca^{2+}]_i$ peaks. High K^+ was used at the end of the experiment to confirm cell viability.

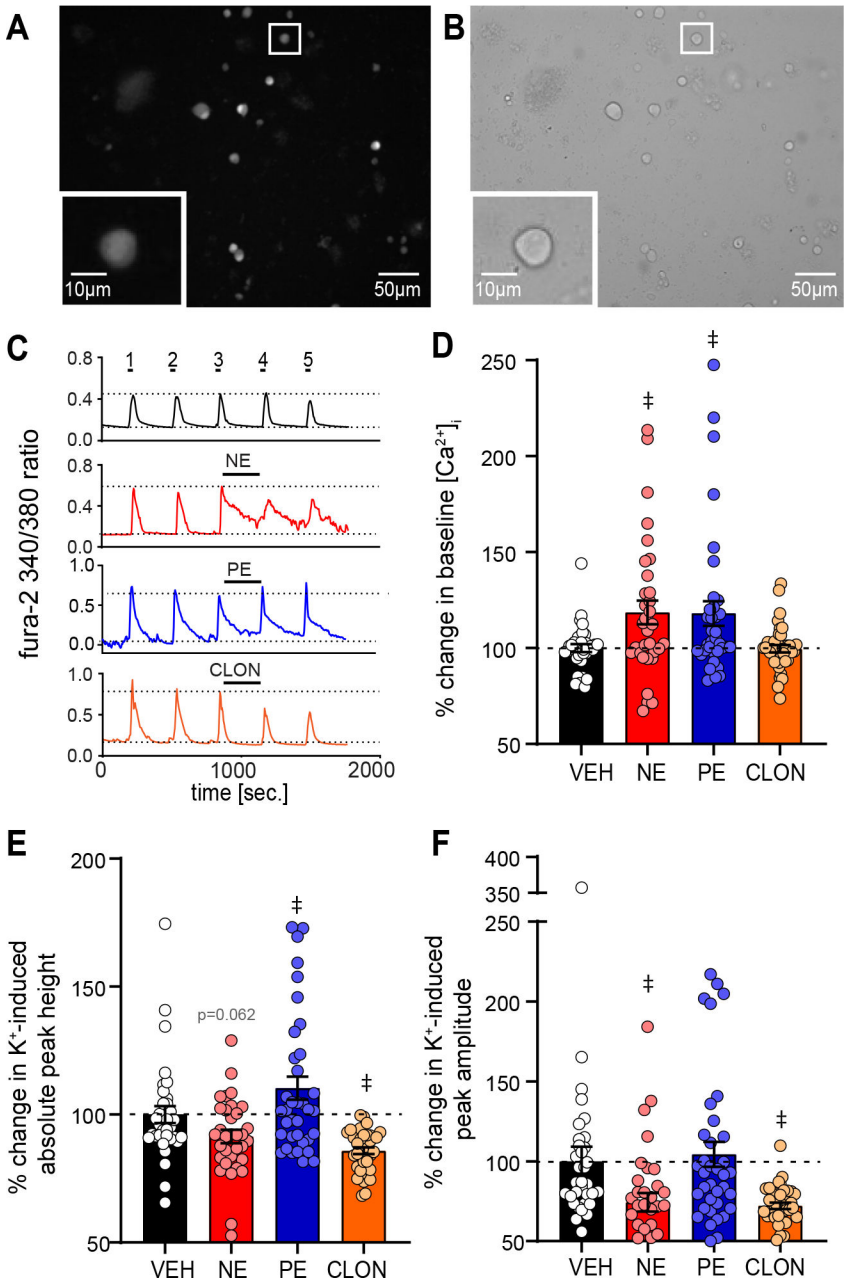

Figure 2. NE increases baseline $[Ca^{2+}]_i$ in between depolarization induced $[Ca^{2+}]_i$ peaks via α_1-AR activation.

***A,B*:** Example of isolated PVN neurons, 2 h after dissociation, under (*A*) 380nm excitation of fura-2 and (*B*) bright field. Inset shows a zoomed representative image of a recorded neuron. ***C*:** Example 340/380 ratios from single representative neurons over time from PVN neurons during repetitive high K^+ depolarization (5X, 20 s each) intermittent with washes (imaging aCSF, 5X, 5 min). The third wash was with aCSF vehicle (VEH, black), NE (red), PE (blue), or CLON (orange). Note NE and PE increase $[Ca^{2+}]_i$ between peaks 3 and 4, whereas CLON and aCSF VEH did not alter baseline activity. ***D-F*:** Average percent change in $[Ca^{2+}]_i$ between peaks 3 and 4 normalized to the vehicle (VEH) for (*D*) baseline $[Ca^{2+}]_i$

immediately prior to high K^+ depolarization, (*E*) K^+-induced total peak height, and (*F*) K^+-induced peak amplitude (i.e., total peak height – baseline). *D*: NE significantly increased baseline $[Ca^{2+}]_i$, an effect mimicked by PE but not CLON. *E*: NE had a small, near significant decrease in K^+-induced total peak height. *F*: NE and CLON significantly decrease K^+-induced peak amplitude while PE did not significantly influence amplitude. Dashed line denotes VEH response for each drug combination. Data shown as individual cell responses overlaying mean ± SEM. aCSF VEH n = 34, NE n = 33, PE n = 36, CLON n = 38. ‡ $p \leq 0.05$ *vs.* aCSF VEH by 1-way ANOVA with LSD.

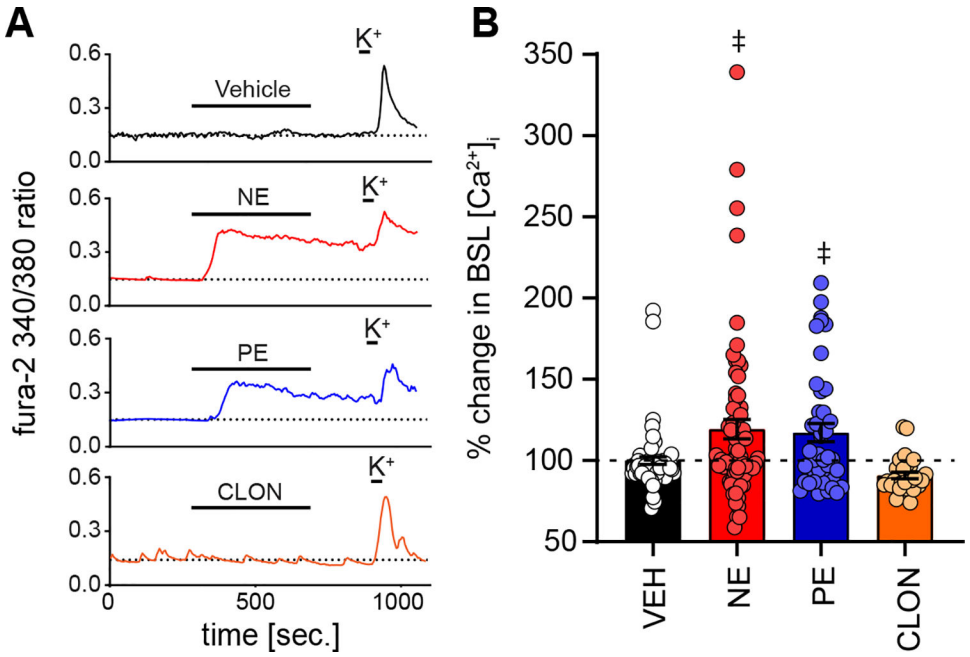

Figure 3. NE increases overall baseline $[Ca^{2+}]_i$ via the α_1-AR pathway.

A: Examples of 340/380 ratios from individual PVN neurons during exposure to 5 min of imaging aCSF (control), then 5 min of treatment, either aCSF vehicle (VEH, top, black), NE (red), PE (blue), or CLON (orange). Note the increase in baseline (BSL) $[Ca^{2+}]_i$ by NE and PE, while CLON only produced a slight, non-significant decrease in BSL. High K^+ at the end of the protocols, and the ensuing calcium peak, ensured cell viability. ***B*:** Average percent change in BSL $[Ca^{2+}]_i$, normalized to the equivalent aCSF vehicle, for aCSF VEH (n = 63), NE (n = 68), PE (n = 42), and CLON (n = 28). NE and PE, but not VEH or CLON, significantly increased BSL $[Ca^{2+}]_i$. Dashed line denotes VEH response for each drug combination. Data shown as individual cell responses overlaying mean ± SEM. $^{‡}p \leq 0.05$ *vs.* VEH by 1-way ANOVA with LSD.

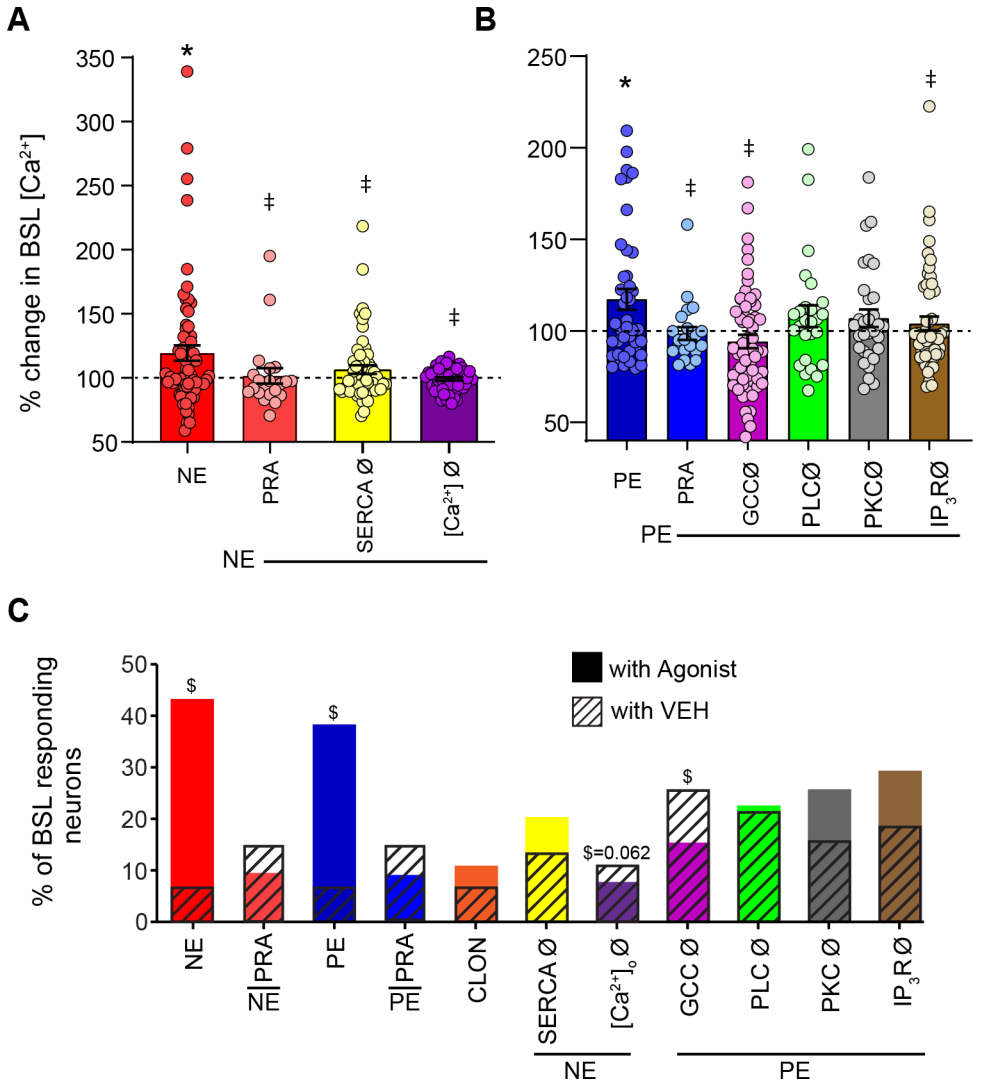

Figure 4. The α_1-AR mediated increase in baseline $[Ca^{2+}]_i$ is depends upon external and internal sources.

A: Average percent change in baseline (BSL) $[Ca^{2+}]_i$ normalized to the equivalent vehicle for NE alone (n = 68), or during PRA block (n = 21), SERCA Ø (n = 59) or $[Ca^{2+}]_o$ Ø (n = 52). Note PRA block and $[Ca^{2+}]_o$ Ø significantly eliminated the increase by NE, and SERCA Ø significantly attenuated NE's effect, which were also not significantly different from their equivalent blocker alone vehicles. ***B***: Average percent change in baseline (BSL) $[Ca^{2+}]_i$ normalized to the equivalent vehicle for PE alone (n = 42), or PE during PRA block (n = 22) or GCC Ø (n = 60). PRA block eliminated the augmentation of $[Ca^{2+}]_i$ by PE. GCC Ø significantly attenuated PE's effect and was not significantly different from its' equivalent vehicle. Also shown is PE in the presence of PLC Ø (n = 26), PKC Ø (n = 31), and IP_3R Ø (n = 53). PE in the presence of the three blockers were not different from their equivalent blocker vehicles. IP_3R Ø was significantly different from PE alone. For A and B, * $p < 0.05$, NE or PE *vs.* its aCSF vehicle from Figure 3. ‡$p < 0.05$, PE or NE *vs.* NE or PE in presence of blocker via 1-way ANOVA. Data shown in A & B as individual cell responses overlaying mean ± SEM. Dashed line denotes VEH response for each drug combination. ***C*:** The

percent of neurons that had a BSL response at least one standard deviation above the equivalent average vehicle response; agonist shown in solid color and vehicle shown in hatched bar. Note the large significant increase in the number of responders with NE and PE exposure which is completely abolished by both $[Ca^{2+}]_o$ Ø and GCC Ø, and nearly abolished by PLC Ø. $^{\$}$ $p \leq 0.05$, agonist treatment *vs.* equivalent vehicle by Fishers exact test.

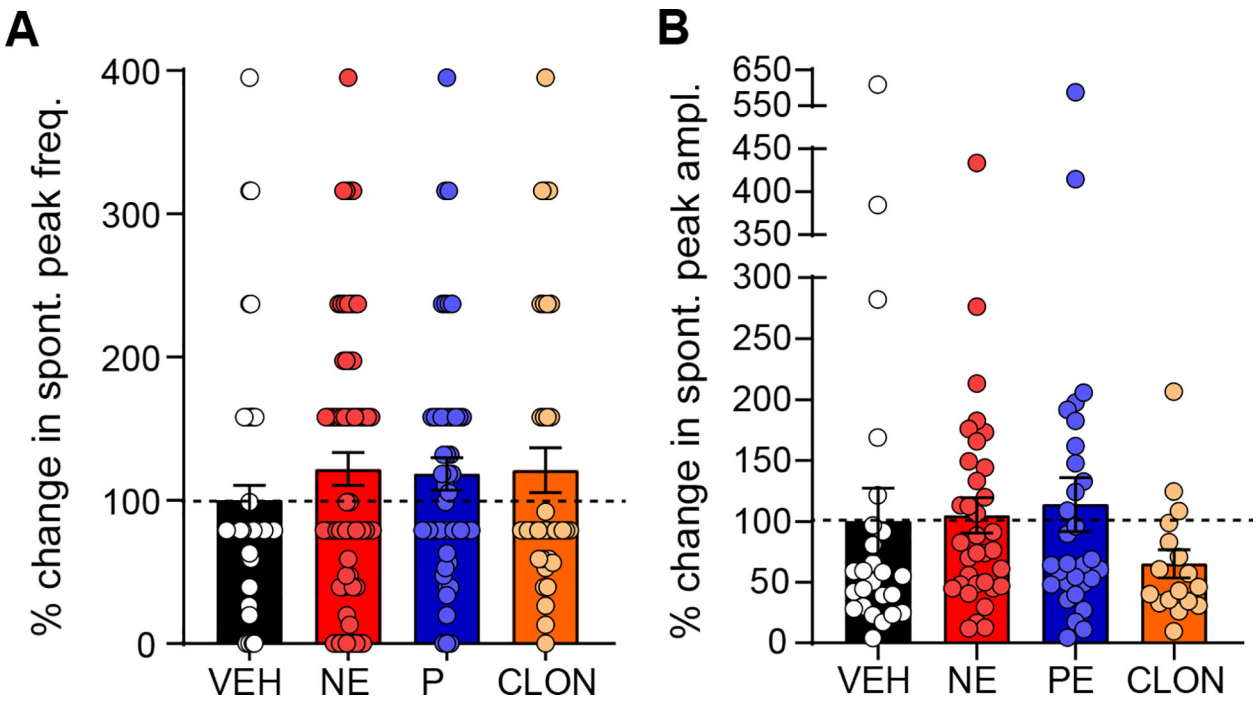

Figure 5. NE does not significantly affect spontaneous peak frequency or amplitude.

A: Percent change of the frequency of spontaneous peaks following NE, PE, and CLON normalized to VEH. No agonist elicited a significant response in frequency. VEH n = 63, NE n = 68, PE n = 42, CLON n = 28. ***B*:** Percent change in the amplitude of spontaneous peaks in response to NE, PE, and CLON, normalized to VEH. Only neurons that had spontaneous events during both the control period and the treatment period were analyzed. CLON non-significantly decreases amplitude compared to VEH (p = 0.7253), NE and PE show little to no change. VEH n = 25, NE n = 34, PE n = 30, CLON n = 17. In panels A & B, dashed lines denotes VEH response for each drug combination, and data shown as individual cell responses overlaying mean ± SEM. *p ≤ 0.05 *vs.* VEH by 1-way ANOVA with LSD.

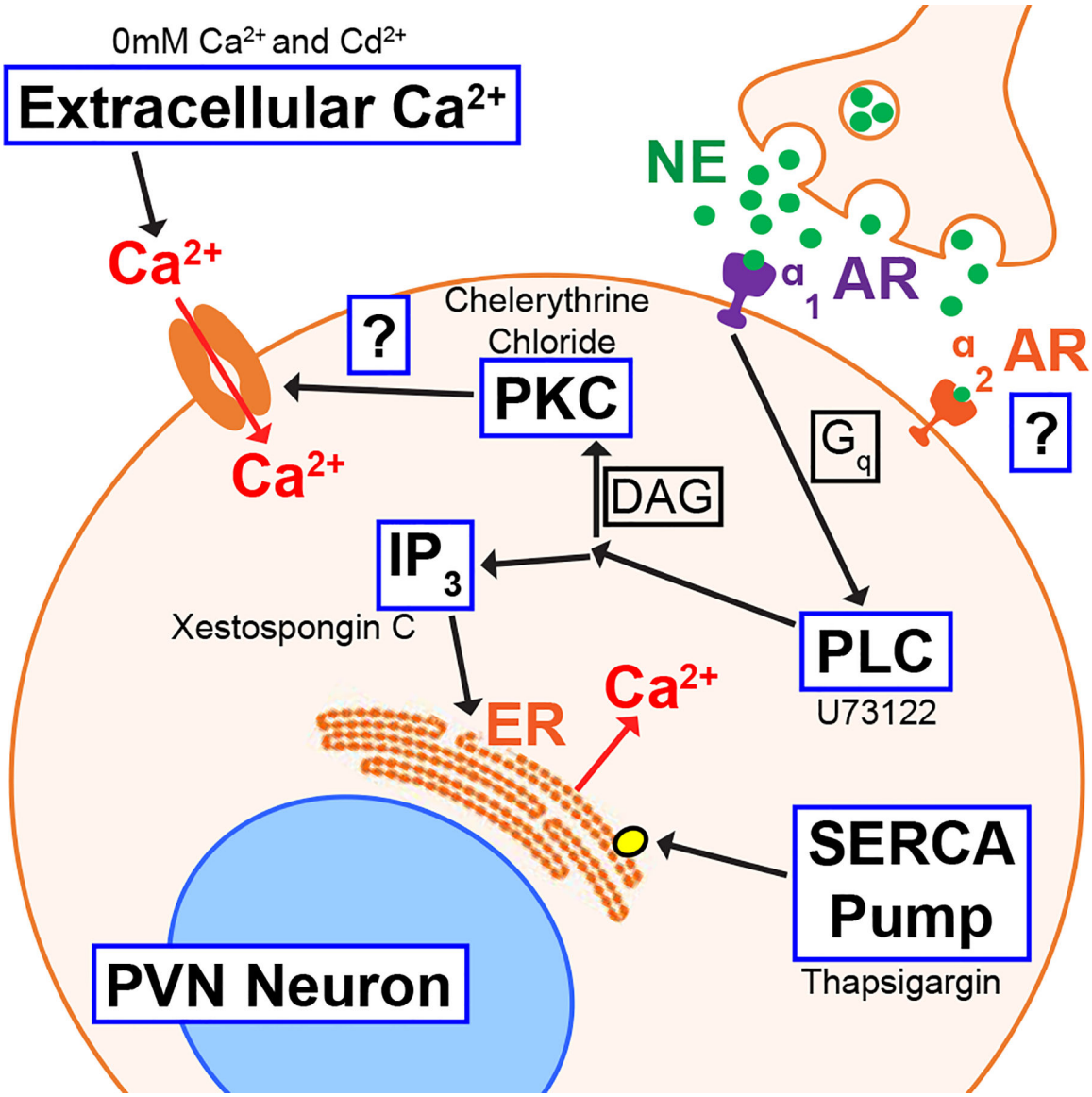

Figure 6. Potential mechanisms of action of NE-elevation of Ca^{2+}.

NE binds to α_1 adrenergic receptors activating PLC via the G_q protein subunit. PLC either activates (1) PKC, resulting in extracellular Ca^{2+} entering the cell, or (2) IP_3, increasing $[Ca^{2+}]_i$ via ER stores. NE also binds to α_2 adrenergic receptors in the PVN, but does not participate in the observed $[Ca^{2+}]_i$ elevation. The tested mechanistic blockers supporting these results are listed adjacent to their pathway.